Understanding steady and dynamic shear banding in a model wormlike micellar solution: supplementary material

Michelle A. Calabrese[†], Simon A. Rogers[ǂ], Lionel Porcar[‡], and Norman J. Wagner[†*]

[†]*Center for Neutron Science, Department of Chemical and Biomolecular Engineering, University of Delaware, Newark, Delaware 19716*

[ǂ]*Department of Chemical and Biomolecular Engineering, University of Illinois Urbana-Champaign, Urbana, Illinois 61801*

[‡]*Institute Laue-Langevin, BP 156, F38042 Grenoble Cedex 9, France*

I. LISSAJOUS-BOWDITCH PROJECTIONS OF LAOS CONDITIONS

The shear stress measured under LAOS for all of the conditions probed using flow-SANS is shown in Figure 1. The Lissajous-Bowditch projections are compared on a normalized basis in order to identify common features of the material response between conditions. The stress response is normalized by the maximum stress (stress at the overshoot), and the strain and shear rate are normalized by the maximum strain and shear rate amplitude, respectively. The elastic Lissajous-Bowditch projections (L) display strong stress overshoots that result in secondary loops in the viscous Lissajous-Bowditch projections (R).

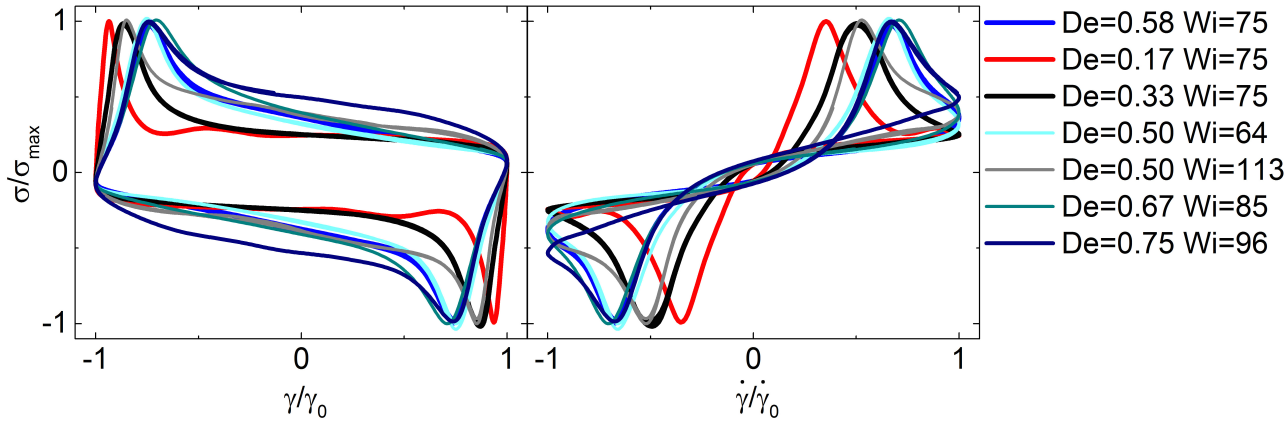

Figure 1: Elastic (L) and viscous (R) Lissajous-Bowditch projections for the LAOS conditions featured, on a normalized strain, shear rate and stress scale. Similar qualitative features are seen in the projections in all conditions, despite significant differences in the shear banding behavior.

One of the biggest differences in the curves is the magnitude of the normalized stress overshoot. At $Wi = 75$, the magnitude of the normalized stress overshoot decreases with increasing Deborah number. When $De = 0.58, Wi = 75$ and $De = 0.50, Wi = 64$, nearly identical normalized Lissajous-Bowditch curves result, which is not surprising considering the similar mechanism of shear banding. However, when $De = 0.50, Wi = 113$, the magnitude of the normalized stress overshoot is roughly the same, but the material does not shear band. The

most significant difference in the Lissajous-Bowditch projection in this condition is the location of the stress overshoot, which occurs at a higher magnitude of the normalized strain. When $De > 0.58$, the normalized stress overshoot remains of similar magnitude and location as at $De = 0.58$, despite that these conditions do not show shear banding. Another distinct difference between the projections of the different conditions is the slope of the normalized stress vs. strain in the region directly following the overshoot. While the lower Deborah numbers show slow changes (low slope), the higher Deborah number conditions show a more drastic decrease in the normalized stress vs. strain (high slope). Again, many of the higher Deborah number conditions show similar normalized responses in this region, despite significant differences in shear banding behavior under LAOS. These qualitative similarities in the Lissajous-Bowditch projections between the shear banding and non-shear banding conditions shows the importance of using spatially-resolved measurements when determining and interpreting dynamic shear banding.

II. UNCERTAINTY ANALYSIS AND REPEATABILITY OF LAOS EXPERIMENTS

To demonstrate the significance of the features of the LAOS stress response, the LAOS experiments were performed for several cycles at the steady alternance state. Additionally, conditions were repeated after a wait time of 30 minutes to ensure the reproducibility of the stress response. The absolute value of the stress response at steady alternance state can be seen in Figure 2 for both conditions, where the error bars represent the standard deviation of the average stress. The overshoots and undershoots observed in condition one are significant aspects of the stress response, as they are not only much larger than the error, but also persistent in both trials. The same is true of the inflection points in the stress response in condition 2. Both stress responses were within error between trials one and two, showing the reproducibility of the LAOS stress response. The uncertainty reported in Table 2 in the text for the maximum stress is the standard deviation (shown by the error bars in Figure 2) around the maximum stress. The uncertainty in the yield strain results from the strain step size between data points in the vicinity of the maximum stress; each test was performed at 256 points per cycle.

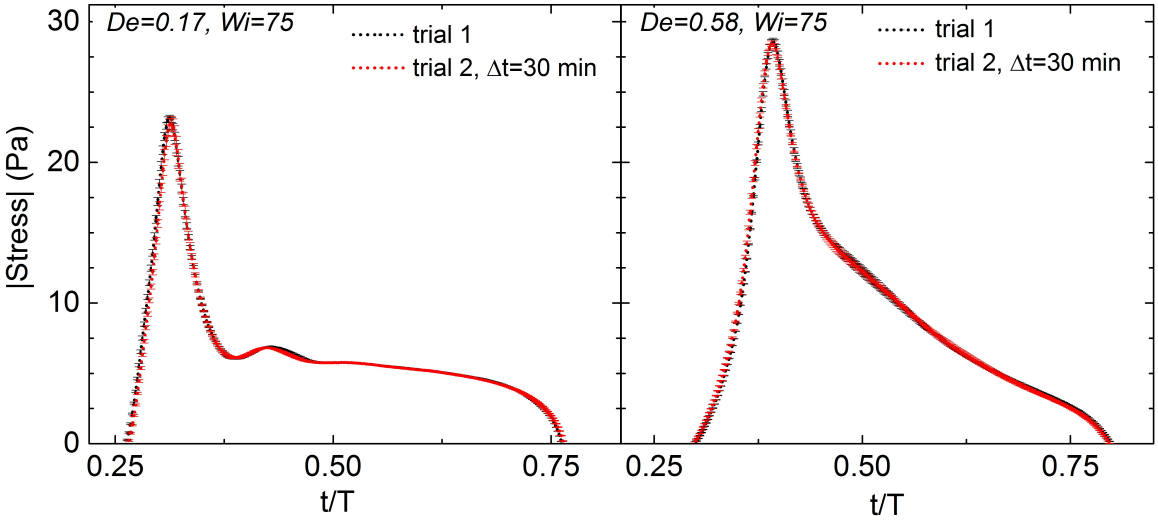

Figure 2: Condition 1 (L) and condition two (R) average stress response and standard deviation over several cycles at steady alternance state for two trials. The stress overshoots, undershoots, and inflection points are significant features of the stress response, when compared to the size of the error bars. Repeated trials show excellent reproducibility. The uncertainty in the stress response is similar in the remaining conditions.

To demonstrate that the LAOS response during 1-2 plane SANS was that of the steady alternance state, the measurements were repeated at the same gap position at two to three different time points after the start of LAOS. This ensures that the material response does not change in time, and that the material does not degrade

during the course of the experiment. These multiple measurements per gap position also ensure that proper statistics are recorded to calculate the alignment factor. The individual SANS measurements are then added together to obtain a final SANS pattern for each time point during the oscillation. The alignment factor curves shown in Figures 8 and 9 are calculated from this final pattern at each time point.

An example of this analysis is shown in Figure 3 for the De=0.58, Wi=75 condition at the inner wall. The measurements at this condition were taken over a total of 20.5 hours, without stopping the oscillation in between measurements. Below, the three trials recorded for $r/H = 0.15$ are shown, where the individual trials are performed over a 16h+ period of time. As this state is the most aligned of all trials between conditions one and two, any changes to the material or instabilities in the system would be most detectable at this condition and position. As Figure 3 clearly shows, the LAOS response is stable and repeatable over this extremely long period of time, which verifies the steady alternance state and the observed over-orientation. Shorter trials at this condition taken in 'kinetic mode' (discussed below) prior to this extended trial confirm that the response is repeatable between multiple trials.

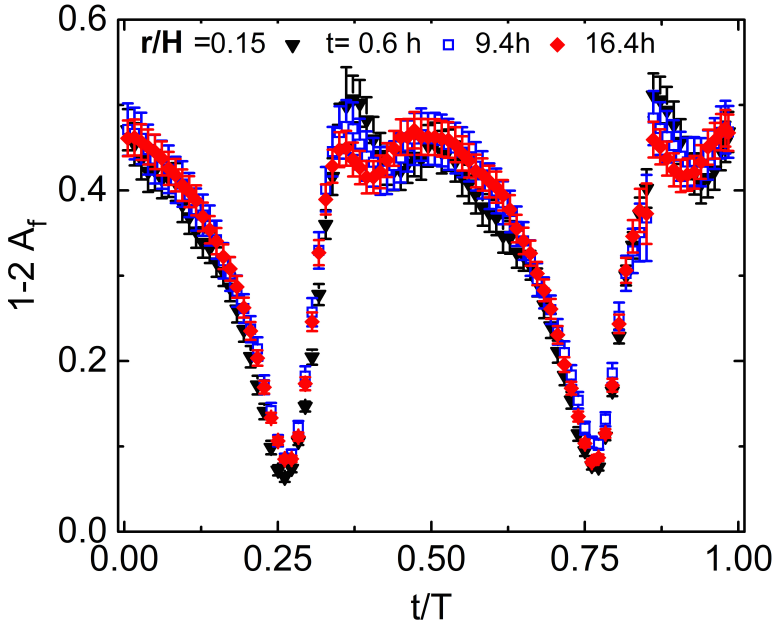

Figure 3: Individual LAOS SANS trials at $r/H = 0.15$ for condition 2. Despite hours of time between individual measurements, the alignment factor response is not significantly different between trials. The individual trials are then added together to calculate the alignment factors shown in Figures 8 and 9.

III. ALIGNMENT FACTOR CALCULATIONS

The alignment factor is normally chosen in the q^{-1}, or rod-like scattering, region of the 1-D scattering. This region is shown between the dotted lines in Figure 4 (L). The chosen q-range for this work, q^*, is highlighted in light blue, and is shown in the top inset for Wi = 75 at r/H = 0.15. The q-range spans $q^* = 0.0199 - 0.0278$ Å^{-1}. The bottom (L) inset shows a sample azimuthal intensity distribution, $I(q^*, \phi)$, from the SANS data for Wi = 75 at r/H = 0.15, which is used to calculate the alignment factor. The bottom (R) inset shows the alignment factor calculation over the full q^{-1} region, using bins of small q-width (designated by the x-error bars). The results are mostly within error of each other. In Figure 4 (R), the 1-2 plane A_f is calculated for the steady shear condition $Wi = 75$ using three different q-ranges within the q^{-1} regime (R). At four of the five gap positions, the alignment is not dependent on the q-range chosen. At r/H = 0.15, the calculated alignment is similar between all q-ranges, indicating that the choice of q-range within the q^{-1} regime does not significantly

affect the results of this work.

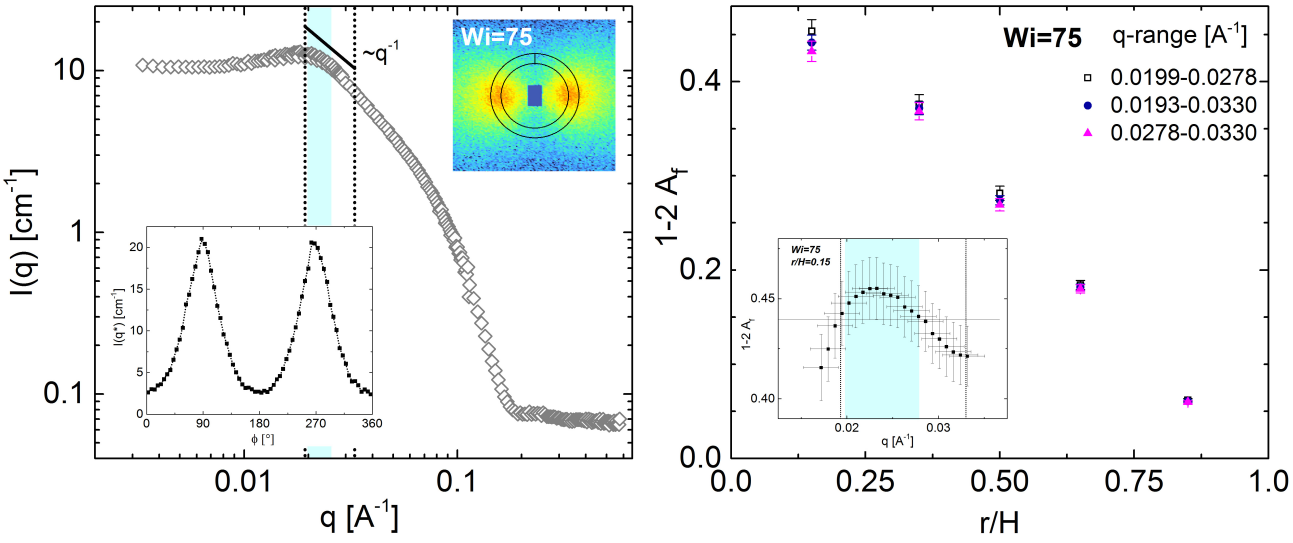

Figure 4: Determination of q-range for alignment factor calculation. (L) The full q^{-1} range is shown in the 1-D scattering between the dotted lines. A sample scattering pattern with the chosen q-range (highlighted in blue) is shown in the top inset ($Wi = 75$, $r/H = 0.15$). In the bottom inset, the azimuthal intensity distribution for the example pattern is shown over q^*. (R) Steady shear 1-2 plane A_f at $Wi = 75$ for our chosen q-range (open squares), the full q^{-1} range (circles), and the second half of the q-range (triangles). At all but r/H = 0.15, the A_f is independent of chosen q-range, indicating that the alignment results are not highly sensitive to choice of q-range. Inset: alignment factor calculated across the relevant q-range in small q-increments (x-error), where the chosen q-range is highlighted in blue. Most of the points across the range are within error of each other.

The alignment factor for all LAOS and steady shear tests was calculated in the ILL GRASP software, as given by Equation 3 in the text. The alignment factor was calculated over the mentioned q^* range using 10° azimuthal bins to determine $I(q^*, \phi)$. Results were identical within error when 5° bins were used; however, these calculations had a higher uncertainty due to the smaller azimuthal bin size and therefore lower neutron count per bin. From GRASP, the error in $I(q^*, \phi)$ was determined based on the neutron count, detector efficiency and resolution, among other factors. This error was then propagated through the alignment factor calculation to determine the uncertainty associated with each alignment factor. The data in conditions one and two was taken with a 0.1 mm slit and was recorded in the ILL 'list mode,' where each neutron is time stamped. This provides the greater temporal resolution seen in these conditions (more data points and alignment factors per t/T), as the data can be processed at any chosen time width. Significantly longer count times were used in these experiments, leading to the lower uncertainty reported in the alignment factor. The data in the other five conditions was taken with a 0.3 mm slit and was recorded using the ILL 'kinetic mode.' In this mode, the temporal bin width is chosen in advance, leading to the fewer alignment factor points per cycle in these tests. Due to time constraints, the experiments were performed for significantly less time, which leads to the higher uncertainty in the alignment factor calculations. The neutron count at each position for the latter five experiments is approximately one-third of the neutron count at each position for the primary two conditions. To ensure that the temporal resolution did not affect the results, the data from conditions one and two was re-processed with the same temporal bin width as the latter conditions; no significant differences in alignment were observed.

IV. TIME DEPENDENCE OF THE 1-2 PLANE ALIGNMENT FACTOR

Time-resolved 1-2 plane SANS measurements were taken at $Wi = 75$ upon shear startup, with the slit translating between positions without ceasing shear. The material response reached steady state within ≈350 s, in good

agreement with our rheo-SANS measurements at $Wi = 75$, and remained at steady state at all $t > 350$s. The alignment factor measurements are shown in Figure 5. The startup of shear began when the slit was located at r/H = 0.15 (inner wall). The Δt of 900 s for $r/H = 0.15$ corresponds to an absolute time starting at $t = 0$ s and ending at $t = 900$ s. As seen in Figure 5, the dotted vertical line when $r/H = 0.15$ indicates the time for the material response to reach steady state after the startup of shear (350 s). At $r/H = 0.15$, at absolute times greater than 350 s, the alignment factor is fairly constant with no significant fluctuations. There are also no significant fluctuations of the alignment factor when $r/H = 0.35$. The absolute time of the experiment at $r/H = 0.35$ corresponds to $t = 3600$ s to $t = 4500$ s after shear startup. Similarly, at $r/H = 0.50$, there are also no significant fluctuations of the alignment factor during the measurement. The absolute time of the experiment at $r/H = 0.50$ corresponds to $t = 1800$ s to $t = 2700$ s after shear startup.

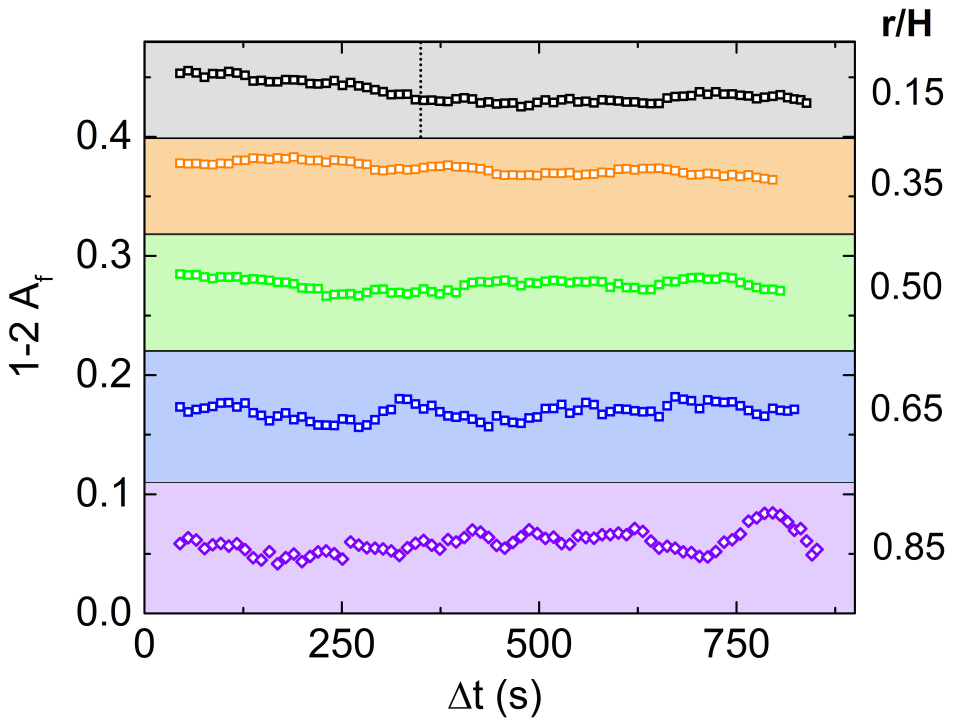

Figure 5: 1-2 plane A_f fluctuations based on gap position after shear startup at $Wi = 75$. The dotted vertical line where $r/H = 0.15$ indicates the time after shear startup for the response to reach steady state, in good agreement with 1-3 plane A_f results. The alignment factor in time is fairly constant at $r/H \leq 0.5$; fluctuations occur at $r/H = 0.65, 0.85$, indicating the proximity of these measurements to the shear band interface.

At $r/H = 0.65$, a different trend in the steady-state alignment factor is observed than at the previous three gap positions. Here, the alignment factor exhibits weak fluctuations at steady-state that are similar to those observed in the 1-3 plane alignment factor at steady-state (data not shown). These fluctuations are likely a result of the shear banding response, which can lead to fluctuating rheological responses and/or a fluctuating shear band interface. The absolute time of the experiment at $r/H = 0.65$ corresponds to $t = 2700$ s to $t = 3600$ s after shear startup. At r/H = 0.85, a similar fluctuating alignment factor response is observed, with even more pronounced fluctuations than are observed at r/H = 0.65. The absolute time of the experiment at $r/H = 0.85$ corresponds to $t = 900$ s to $t = 1800$ s after shear startup. As the steady-state alignment factor response fluctuates at both $r/H = 0.65$ and $r/H = 0.85$, it is likely that the shear band interface is located in between these two gap positions. With the 0.1 mm slit, the r/H = 0.65 position covers r/H = 0.6 to 0.7 and r/H = 0.85 covers r/H = 0.8 to 0.9, so we infer that the interface is between r/H = 0.7 and 0.8. This proposed interface location is in good agreement with the calculation of α = 0.75 at Wi = 75.

V. COMPARISON OF TWO LAOS CONDITIONS

The difference in the shear banding behavior between conditions one and two can be further explained when the alignment between the two conditions is directly compared. Figure 6 shows the alignment factor as a function of gap position for both conditions, where condition one (De = 0.17, Wi = 75) is shown with solid lines and condition two (De = 0.58, Wi = 75) is shown by data points.

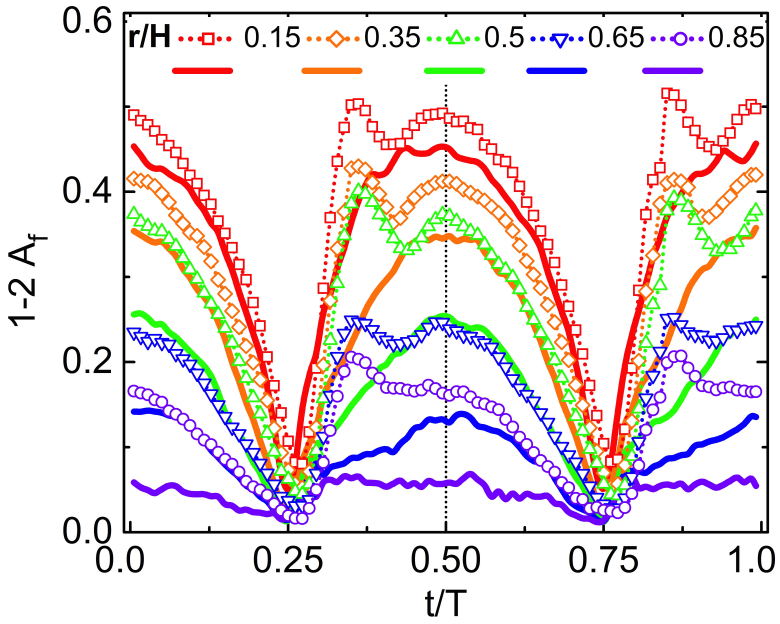

Figure 6: 1-2 plane A_f as a function of t/T and r/H for both conditions. Condition one (De = 0.17, Wi = 75) is shown with solid lines whereas condition two (De = 0.58, Wi = 75) is shown with data points. With decreasing $|\dot{\gamma}|$ ($0 \leq t/T \leq 0.25$, $0.5 \leq t/T \leq 0.75$), A_f is similar between conditions at r/H =0.15 and 0.35. When r/H $\geq$ 0.5, the alignment factor deviates, suggesting a different mechanism of shear banding.

In Figure 6, the alignment in regions of increasing shear rate magnitude ($0.25 \leq t/T \leq 0.5$, $0.75 \leq t/T \leq 1$) is significantly different between the two conditions, resulting from the differences in cycle time and material relaxation during LAOS. A different trend, however, is observed when the regions of decreasing shear rate magnitude are examined. In these regions ($0 \leq t/T \leq 0.25$, $0.5 \leq t/T \leq 0.75$), the alignment factor is nearly identical between the two conditions at the inner-most position, and is similar when r/H = 0.35, suggesting a similar material structure. This again suggests that the material at the inner wall has to relax much less to reach steady state during shear banding than the material at the outer wall. When $r/H \geq 0.5$, the magnitude of alignment differs. In fact, the alignment at r/H = 0.5 for condition two (upward triangles) is now nearly identical to the alignment of condition one at r/H = 0.35. Further, the alignment for condition two at r/H = 0.65 (downward triangles) and 0.85 (diamonds) in this region now nearly identically follows the condition one alignment at r/H = 0.5 and 0.65, respectively. The different alignment trends between the conditions enable us to identify different mechanisms of shear banding under LAOS. Such results highlight the importance of using spatially-dependent structure measurements to elucidate the material response, as opposed to bulk rheology or 1-3 plane SANS alone. While both samples exhibit large stress overshoots and qualitatively similar LAOS curves, one exhibits more significant shear banding and a metastable structural state, whereas the other is able to access stresses below those of the measured steady shear flow curve. Without spatially-resolved measurements, shear banding under LAOS could be hypothesized in both conditions from model predictions but the mechanism of shear banding could not be elucidated.